Available online at www.sciencedirect.com
SCIENCE DIRECT®
Surface Science 574 (2005) 1–16
SURFACE SCIENCE
www.elsevier.com/locate/susc

Adsorption of CO on $PtBi_2$ and PtBi surfaces

Melania Oana, Roald Hoffmann *, Héctor D. Abruña, Francis J. DiSalvo

Cornell University, Department of Chemistry and Chemical Biology, Baker Laboratory Ithaca, NY 14853-1301, USA

Received 7 July 2004; accepted for publication 23 September 2004
Available online 3 November 2004

Abstract

Approximate molecular orbital calculations have been applied to explain the low CO poisoning effects observed at $PtBi_2$ and PtBi electrodes. The bonding patterns for chemisorption of CO on the surfaces of Pt–Bi bulk alloys and pure Pt surfaces are quite similar. The major difference is not induced through much Pt–Bi bonding, but indirectly, by raising the Fermi level of the system, so that the C–O π^* levels become practically filled upon interaction. This results in much lower adsorption energies than in the metallic Pt case, in accordance with experimental data. The calculations also imply C–O bond dissociation on the surface, a phenomenon not supported by experiment. CO adsorption at Pt–Pt bridge site (possible only on PtBi) is favored relative to atop chemisorption.

Keywords: Molecular orbital calculations; Chemisorption; Carbon monoxide; Platinum; Bismuth; Intermetallic compounds

1. Introduction

There is no molecule whose adsorption on various metal surfaces, pure metals or alloys has been studied more extensively, both theoretically [1–5,16–32,40–43] and experimentally [6–15,33–39,44–49], than CO. The references cited are but a selection of the published work in this field. Yet interest in CO chemisorption continues unabated, one reason today being its role in the development of better fuel cell catalysts. CO is generated in the process of electro-catalytic oxidation of small organic molecules (often via dissociative chemisorption) and it causes substantial poisoning of the active sites on precious metal catalysts, especially Pt [50–55]. Modification of the metal surface by adatoms, adlayers, all the way to surface and bulk alloys can lead to improved catalytic properties and tolerance to CO [50,53–55]. For many alloyed systems, the CO adsorption energies also decrease considerably [40,41,44–46,49]. Still, a significant shortcoming of these catalysts is that their surface structure is not well characterized and may change in time.

* Corresponding author. Tel.: +1 607 255 3419; fax: +1 607 255 5707.
E-mail address: rh34@cornell.edu (R. Hoffmann).

0039-6028/$ - see front matter © 2004 Elsevier B.V. All rights reserved.
doi:10.1016/j.susc.2004.09.045

Recently, Abruña and co-workers [56] have studied the electro-oxidation of formic acid on the surface of the ordered intermetallic compounds $PtBi_2$ and PtBi. In the case of PtBi, their experiments show superior catalytic properties in the oxidation of HCOOH, with respect to Pt (a more negative onset potential and higher current density), as well as a high tolerance to CO. HCOOH oxidation can take place through a dual pathway mechanism [57,58], shown in Scheme 1. One path goes through a reactive intermediate yielding CO_2 and H_2O; the other one has CO as a stable intermediate that can be oxidized in a subsequent step. This latter path requires more energy (much higher overpotential), which results in a considerable decrease of the efficiency of fuel cell catalysts.

The negligible poisoning observed for electro-oxidation of formic acid on PtBi and $PtBi_2$ can be rationalized by the activation of the reactive pathway at the PtBi electrode, and/or by the low tendency of CO to bind to this surface. Abruña and co-workers proposed that the latter effect is probably largely due to geometrical constraints—Pt atoms being too far apart to allow CO to adsorb in a bridge or 3-fold site. Chemisorption of CO at these sites is often associated with efficient poisoning on Pt surfaces. Nevertheless, electronic considerations should not be ignored as factors in CO binding. Thus, the purpose of this study is to analyze how the classical picture of bonding of CO to transition metals is modified in the case of an intermetallic compound with a p block metal.

As mentioned earlier, the literature regarding CO chemisorption is vast. In general, it points towards a Blyholder—based [59] model of the CO adsorption on transition metal surfaces. This consists of two main interactions: the donation of electrons from the 5σ (and to a lesser extent from 4σ) filled levels of CO to the metal, and the back-donation from the metal into the CO 2π (π*) empty orbitals. Although most of the studies agree with this view, there is much debate as to whether the σ interaction is net repulsive, or indirect (by metal–CO antibonding molecular orbitals being pushed above the Fermi level) [7,24,30,33,60–68]. Also the extent of the 4σ involvement is unclear. The binding depends on the particular system under study and is determined by factors such as the occupancy and the position of the metal d band.

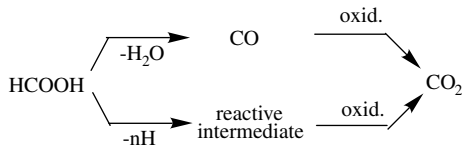

Scheme 1. Dual pathway mechanism for the electrooxidation of formic acid.

In our work on the Pt–Bi intermetallic surfaces, all the calculations were carried out using the tight-binding extended Hückel (eH) method. Though this method does not allow geometrical optimization, nor are its energetics reliable, it is transparent, and capable of explaining electronic effects. Thus, in our analysis we emphasize a qualitative understanding of the phenomena, as a first step in an ongoing investigation of catalysis on intermetallics.

2. PtBi and $PtBi_2$ crystal structures

PtBi has been reported to have an inverse NiAs type hexagonal structure, the lattice constants being $a = 4.340$ and $c = 5.493$ Å [69]. According to Zhuravlev and Stepanova, Bi occupies the $(0,0,0)$ and $(0,0,1/2)$ positions, while the Pt atoms are located at $(1/3,1/3,1/4)$ and $(2/3,2/3,3/4)$. This defines an ideal trigonal prism geometry for Pt and an octahedral environment for Bi, which in addition, has a very short Bi–Bi contact of 2.747 Å. If one counts the Bi–Bi pairs as 4−, Pt would be in a 2+ oxidation state for which the most common geometry is square planar, followed by the octahedral one. Trigonal prismatic coordination is rare for Pt.

Re-analysis of the X-ray powder diffraction data for PtBi by DiSalvo and co-workers led to a better refinement if the Pt and Bi positions were interchanged [56]. Such a structure is more plausible, considering that Pt is then octahedrally coordinated by Bi and that the Pt–Pt distance of 2.747 Å would fall into the normal Pt–Pt bonding range, while for a Bi–Bi bond it is too short. Observed Bi···Bi single bond distances usually vary

between 2.98 and 3.31 Å [70–72]. The Bi–Bi distance in the revised structure is rather long (3.718 Å), but may indicate some weak Bi–Bi interaction. The revised NiAs type structure, suggested by the new work (Fig. 1) was employed in the following calculations.

$PtBi_2$ (Fig. 2a) adopts the pyrite structure, with Pt at the origin and the centers of the cube faces. There are eight Bi atoms per unit cell at (0.3710, 0.3710, 0.3710) and all symmetry equivalent positions [73]. Pt atoms are surrounded by six Bi atoms in a nearly ideal octahedral geometry (best seen in Fig. 2a). Each Bi is coordinated by three Pt atoms, forming a trigonal pyramid, plus another Bi atom at 2.995 Å, thus completing a flat tetrahedron. All octahedra and Bi–Bi bonds are tilted with respect to the crystal axes, and their orientation flips along the three different unit cell axes. The Pt–Bi–Pt angle is 117.6°, which implies that the three Pt atoms and the Bi are almost coplanar.

Another, simpler picture of the $PtBi_2$ structure proved to be very useful in the treatment of the present surface problem. In this view (Fig. 2b), we start with a dilated fcc Pt lattice (a = 6.7014 Å), with Bi_2 dumbbells inserted in a tilted way in the interstitial spaces. This perspective enables a direct comparison with the metallic Pt case (also an fcc lattice, with a = 3.942 Å) and allows one to focus on the electronic effects due to Pt–Bi interactions.

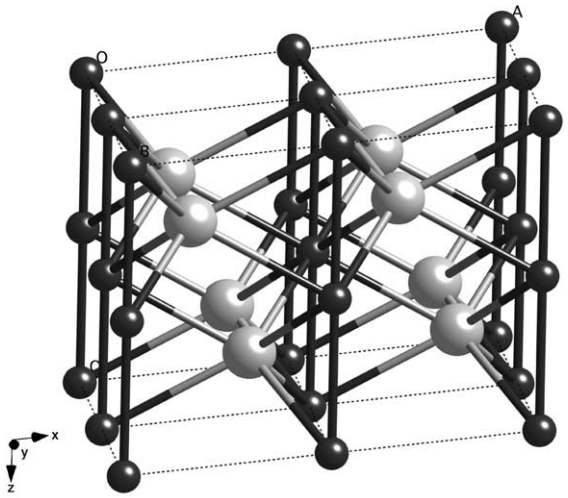

Fig. 1. PtBi structure. Pt (black) forms chains parallel to the c-axis.

3. Methods

All computations were performed at the eH level. For extended 2D and 3D structures, the tight

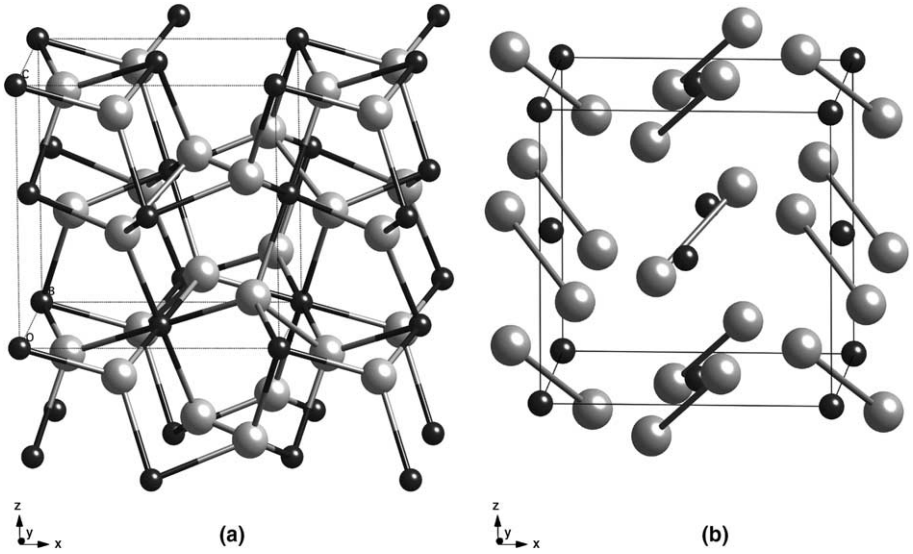

Fig. 2. Different views of the $PtBi_2$ structure: (a) emphasizes the Bi and Pt environments; (b) the Bi–Bi bonds.

binding method as implemented in the YAEHMOP package [74] was employed, while molecular calculations were carried out by the CACAO program [75]. In both cases, the same (default) values of the exponents and H_{ii} parameters were used, as specified in Table 5 in Appendix A.

4. Band structure of $PtBi_2$

Many theoretical investigations—checked against experiment—of the adsorption of small molecules on alloyed transition metals indicate that the major change in alloying consists in an energy shift of the d band position. This effect can be monitored by and scaled with the change in the average center of the d band with respect to the adsorbate levels [29,46,48,76–80]. Unfortunately, the extended Hückel model is not able to capture all the factors that would cause a band shift (for example the charge effects). However, similar reasoning can be applied to the eH calculated density of states (DOS) for different compounds, in order to predict or explain their surface behavior.

Fig. 3 displays the total density of states, DOS and the projection of the d orbitals of bulk Pt, the Pt sublattice of $PtBi_2$ by itself, and the same sublattice in $PtBi_2$. Comparing the right and left DOS one can observe that the center of the d band stays approximately at the same energy.

A seeming anomaly in the DOS of $PtBi_2$ is the very small dispersion of the d band (≈2 eV). Taking into account that part of the spreading comes from the Gaussian functions used to fit the DOS, the remaining d band width is ≈1 eV. A good estimate of the Gaussian widening is given by the picture in the middle panel, where one can clearly see the nearly non-interacting d, s, and p orbitals of Pt atoms, the closest Pt–Pt distance being 4.739 Å.

The small Pt 5d bandwidth in $PtBi_2$ is no doubt due to the large Pt–Pt separations. The projected Pt d orbitals in $PtBi_2$ also show relatively little mixing with the Bi s and p orbitals. Formal electron counting for $PtBi_2$ gives 4+ as the oxidation number for Pt, and 2− for each Bi in the Bi_2^{4-} pairs. The Pt d^6 configuration is consistent with its octahedral coordination, since the crystal field splitting of the d levels for this geometry is usually three (t_{2g}) below two (e_g). Even if Bi is not known as a good ligand, one would expect to see some memory of the t_{2g}–e_g splitting in an octahedral geometry and a larger degree of Bi–Pt d interaction than revealed by its bandwidth. Such crystal field splitting is not apparent in $PtBi_2$.

To clarify the issue, molecular extended Hückel calculations were performed on a ideal octahedral $PtBi_6$ molecule (the charge is unimportant in eH; the electron occupation shown in Fig. 4 is for $Pt^{4+} + 6Bi^{3-}$), keeping the same Pt–Bi distance as in $PtBi_2$: 2.771 Å. The Pt + 6Bi interaction diagram

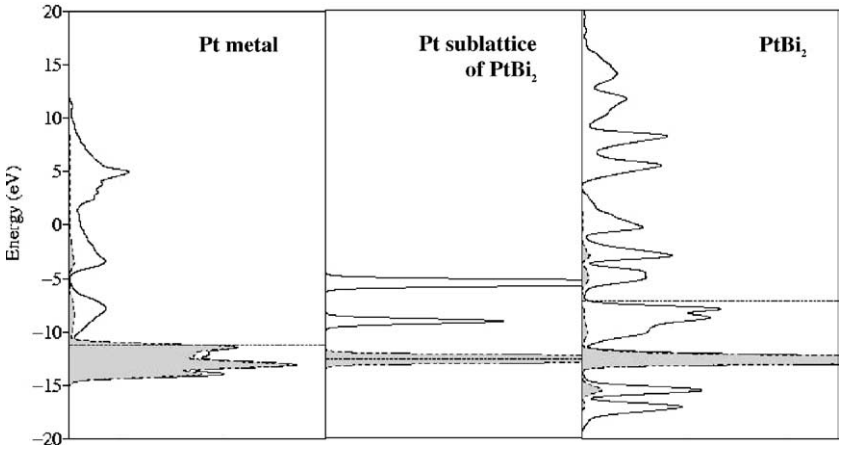

Fig. 3. Total DOS (solid line) and the contribution to the DOS of Pt d levels in Pt metal (left), isolated Pt sublattice of $PtBi_2$ (middle) and $PtBi_2$ (right).

and the $PtBi_6$ molecular orbitals (MOs) are drawn in Figs. 4 and 5. Among the $PtBi_6$ electronic levels there are two t_{2g} and three e_g sets, so it is not that easy to identify those involved in the classical ligand field argument. The $1t_{2g}$ MOs are mainly non-bonding with 68% Pt contribution, while the $2t_{2g}$ set is the π antibonding combination with only 32% Pt contribution. Let us tentatively identify $1t_{2g}$ as the "metal" t_{2g} set. Two of the e_g sets are formed from the Bi s and p orbitals; the Pt e_g set lies energetically in-between the Bi ones. The $2e_g$ MO's (70% Pt contribution) are engaged in a three-orbital interaction with Bi s and p e_g orbitals. The final crystal field splitting, e_g–t_{2g}, focusing on $2e_g$ and $1t_{2g}$, is just 0.33 eV. Since Bi has filled orbitals at lower and also at higher energy than the Pt d levels, one can view $PtBi_6$ as an intermediate case, on the way to an "inverse" crystal field splitting. Whether t_{2g} is below e_g (the usual case) or above it (an "inverse" crystal field) depends on the energies of the interacting ligand levels relative to the d block of Pt.

We also looked at another model, in which the Bi neighbors of Pt were modeled by BiH_3 ligands, i.e. we calculated $Pt(BiH_3)_6^{4+}$. If one looks for the orbitals most heavily weighted on Pt, one finds the relevant t_{2g} around −12.6 eV, and the e_g at −13.4 eV. Thus in this model there is a small inverse crystal field splitting of 0.8 eV.

Gaining confidence from the molecular analysis that the narrow d band in $PtBi_2$ represents only an accidentally small crystal field splitting, and is not evidence of a lack of orbital interaction, we can move on to the actual surface problem.

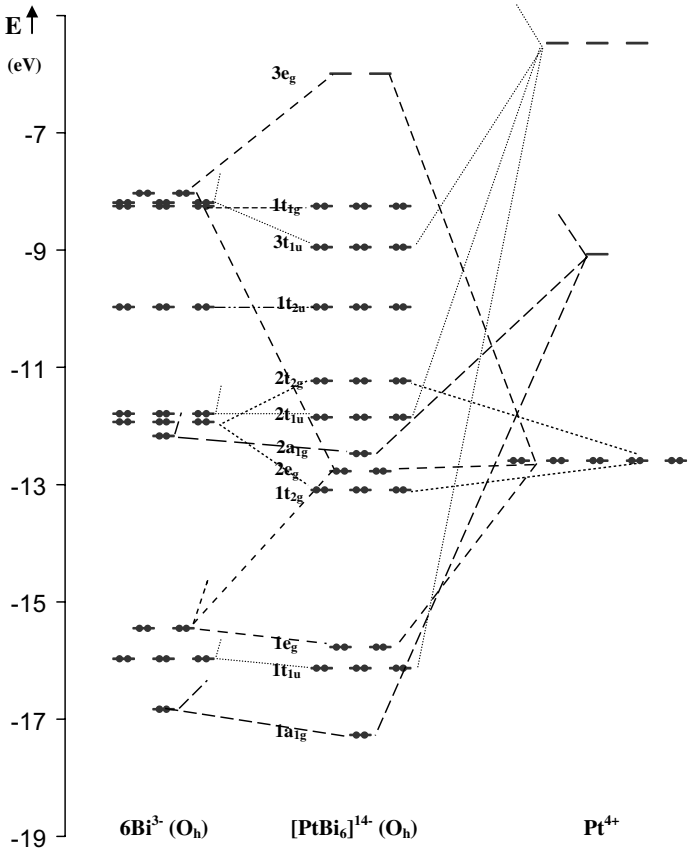

Fig. 4. Interaction diagram for $PtBi_6$ octahedron from Pt^{4+} and $6Bi^{3-}$ electronically stable fragments. Two higher-lying MOs, $4t_{1u}$ and $3a_{1g}$ do not appear in this energy window.

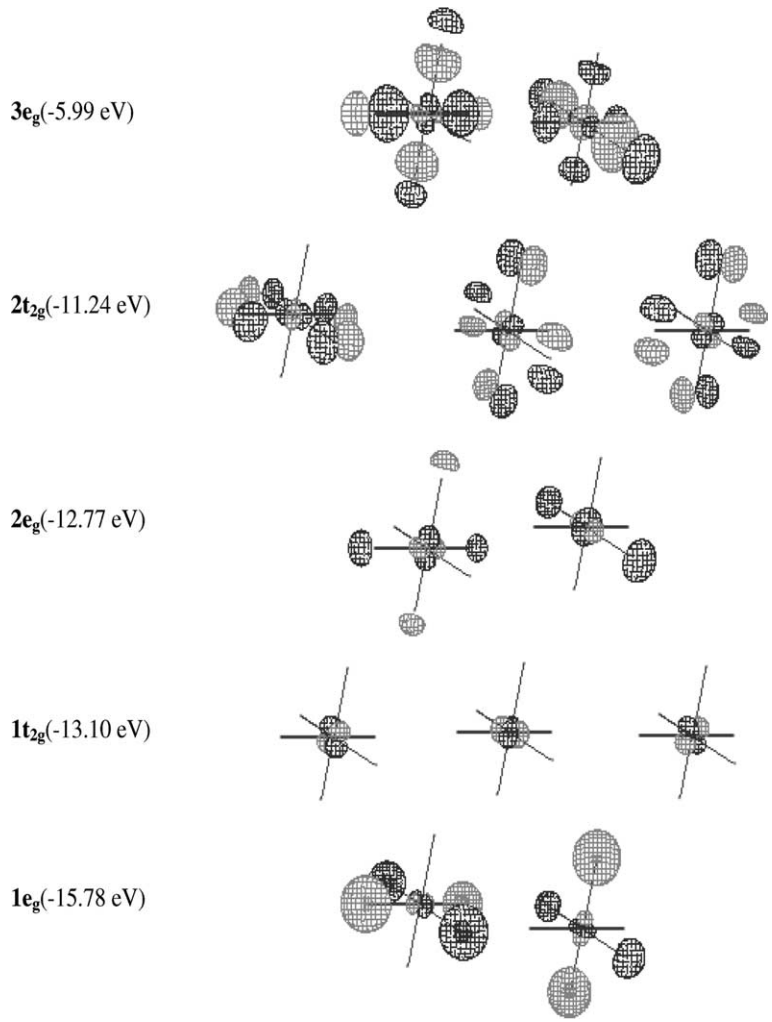

Fig. 5. Molecular orbitals of the $PtBi_6$ octahedron: $1e_g$, $1t_{2g}$, $2e_g$, $2t_{2g}$, $3e_g$ (from bottom to top, in order of increasing energy).

5. $PtBi_2$ and PtBi surfaces

The $PtBi_2$ and PtBi electrodes used in experiments by Abruña and co-workers [56] are polycrystalline. Thus CO adsorption has to be studied for a range of surfaces of both $PtBi_2$ and PtBi. Little appears to be known about the surfaces of Pt–Bi intermetallic compounds or their reconstruction(s), if any. That is why we looked for guidance at two compounds with the same lattice type as $PtBi_2$ and PtBi: FeS_2 and NiAs, respectively. We then considered for adsorption on $PtBi_2$ and PtBi the surfaces with the same indexes as the most stable surfaces of the corresponding isostructural compounds. These are: (1 0 0), (1 1 0), (1 1 1), (2 1 0) for $PtBi_2$ and (0 0 1), (1 0 0), (1 1 0) for PtBi. Only the Pt-rich surfaces of a given index were taken into account. It seemed to us that the lone pairs on Bi would preclude CO chemisorption at Bi ions. Further calculations confirmed this supposition.

In a first step, only the adsorption of CO directly atop a Pt atom on the surface was considered, since tilted CO adsorption is reported just for high coverages [9,81–85]. Calculations were also done for CO in a bridge site on PtBi, the only

multicenter adsorption case possible geometrically. In order to minimize CO–CO intermolecular interaction on the surface and not to deal (initially) with coverage effects, we approached only one CO per surface unit cell. The large resultant lattice constants assure minimal lateral interactions. The Pt–C and C–O distances were chosen as 1.85 and 1.15 Å (from LEED data [86,87]), other experimental and theoretical studies on adsorption of CO on Pt and Pt alloys giving bond distances around the same values [1,2,5,46,62].

Building on the connection between the metal Pt (fcc) and the $PtBi_2$ structures, emphasized in Fig. 2b, calculations for the adsorption of CO on the (0 0 1), (1 1 0) and (1 1 1) surfaces of bulk Pt were carried out too. This provided a reference point for the $PtBi_2$ + CO system and made possible the comparison, within the same framework, of the adsorption phenomena on the two different types of surfaces. Furthermore, in order to distinguish the effect of increasing the distance between Pt atoms in the lattice from that due to the Pt bonding to Bi atoms, the same calculations were repeated for the Pt sublattice of $PtBi_2$. The number of Pt atoms in the Pt slabs (both, bulk metal and sublattice), the surface unit cells and the adsorption sites were kept the same as in the corresponding $PtBi_2$ cases.

6. CO chemisorption on $PtBi_2$

6.1. Bonding analysis

Fig. 6 depicts the $PtBi_2$ surfaces used for calculations and the all the non-equivalent adsorption sites for each surface. The conclusions were similar for all the cases studied; the following discussion will focus on the (0 0 1) surface as a representative example.

On the right-hand side of Fig. 7, the contribution of the CO fragment MOs to the total DOS of the (0 0 1) $PtBi_2$ + CO system is shown. From a comparison with the energies and bandwidths of the same MOs in an isolated CO layer (left, bandwidths are not real, but due to Gaussian "broadening" in DOS calculation), one can trace the adsorbate–Pt interactions.

The 4σ MO interacts weakly (very small downshift in energy), the main σ-type interaction being due to the 5σ level. There are two Pt orbitals that can interact with CO 5σ, d_z^2 and p_z. The result is a three orbital-type interaction: d_z^2 mixes into the 5σ band (and a little into 4σ), while p_z levels are pushed up, forming mainly the antibonding combinations. The p_z band peak around −6.5 eV in a $PtBi_2$ slab is found after adsorption at 30 eV (not shown in Fig. 7).

The CO π band does not show any obvious changes, while the π* levels interact to a large extent. The π* band spreads out significantly to higher energies and one can observe its mixing into the Pt d band.

In analyzing the chemisorption of CO on a $PtBi_2$ or PtBi surface, it is useful to have as a reference point what happens to CO on a pure Pt surface. This has been studied in depth before [1,5,24,62], so we abbreviate the discussion to some points of interest here. Crystal Orbital Overlap Population (COOP) [88] curves in Figs. 8 and 9 provide information about the C–O and Pt–C bond changes, respectively, upon adsorption. The C–O COOP for a CO single layer is given for comparison (Fig. 8, 3rd panel). This is calculated for essentially isolated CO molecules, kept for convenience in the same geometry as on (0 0 1) $PtBi_2$. However, any other arrangement with large intermolecular distances would give the same results.

Let's look first at CO on a (0 0 1) surface of pure Pt (Fig. 8, left). Besides the shift in energy and dispersion of the levels due to the orbital interactions discussed above, the relative bonding character has changed a little: the 5σ band (shifted down in energy) has somewhat greater C–O bonding character, 4σ—smaller. The broader, filled C–O antibonding band centered around −12.5 eV corresponds to CO π* levels that mix into the Pt d band.

The COOP for the Pt–C bond is in some aspects the inverse of the C–O one. The 4σ, 5σ and π bands also have Pt–C bonding character, but the relative contribution to bonding is reversed (relative to C–O), proportional to the Pt interaction in those bands with CO. The band centered at −12.5 eV is Pt–C bonding; this is the metal–CO π* interaction. The first Pt–C levels that are antibonding are located above −9 eV and they are

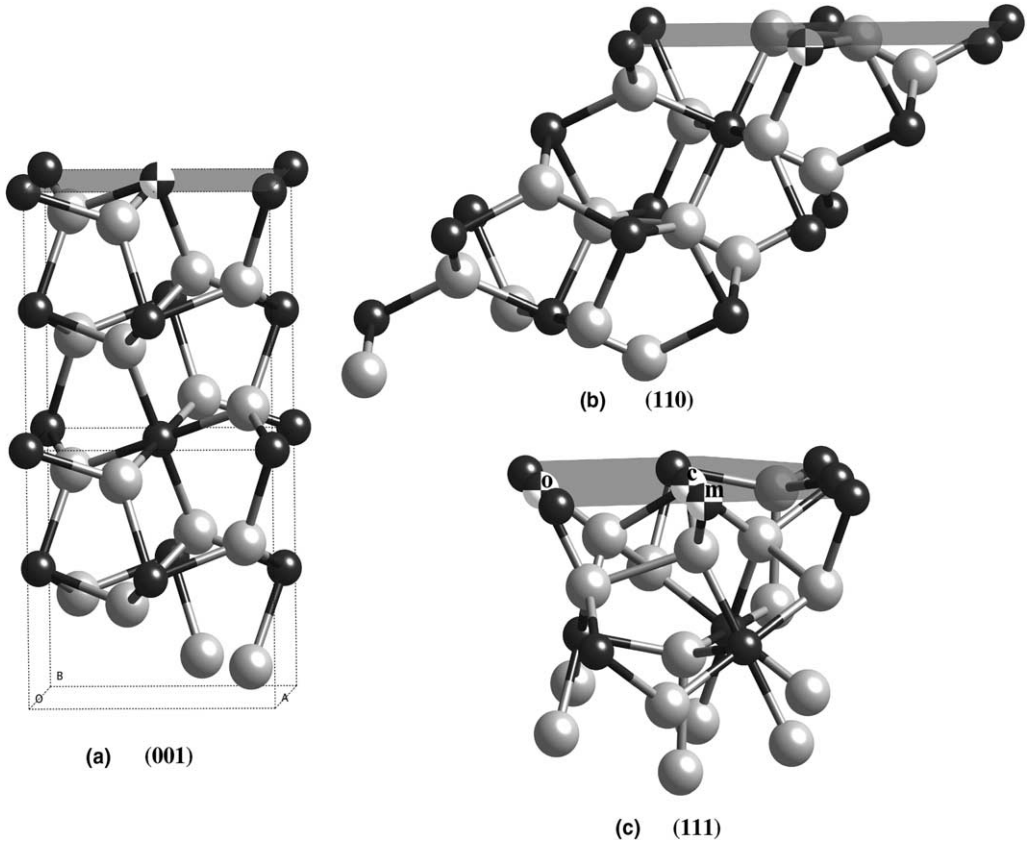

Fig. 6. Actual slabs (one *xy* unit cell) and different atop adsorption sites (quarter split atoms) chosen for the atop adsorption of CO on $PtBi_2$ surfaces (gray plane): (a) (0 0 1), (b) (1 1 0), (c) (1 1 1)—*o*, *m* and *c* are the notations for the three non-equivalent sites.

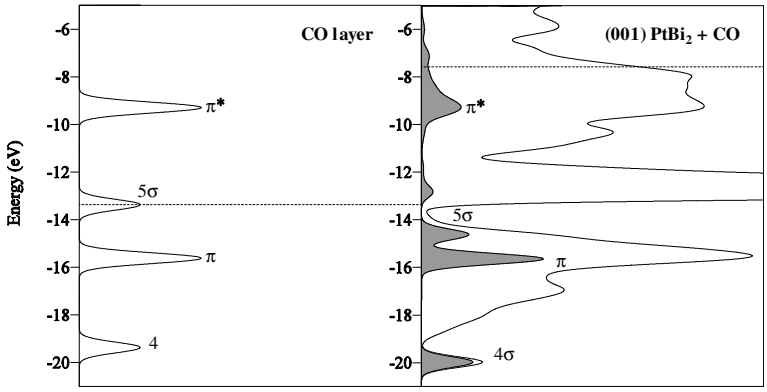

Fig. 7. DOS of the isolated CO layer (left), of (0 0 1) $PtBi_2$ + CO system (right, solid line) and contributions to the DOS of the adsorbed CO levels (right, dashed line and dark area).

combinations of the highest levels involved in the σ type interaction, Pt p_z.

The next step in the analysis is to "take apart" the Pt atoms and look at the hypothetical case of

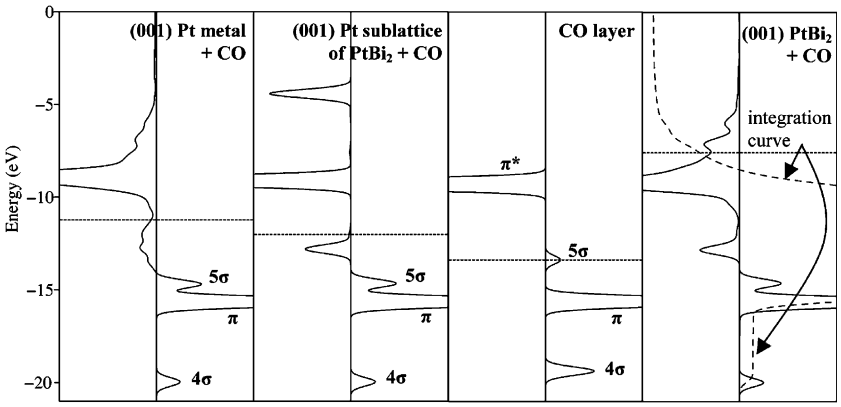

Fig. 8. COOP for the C–O bonds in (0 0 1) Pt metal + CO (left), (0 0 1) Pt sublattice (of $PtBi_2$) + CO (2nd panel), CO isolated layer with the same geometry as on $PtBi_2$ (3rd panel) and (0 0 1) $PtBi_2$ + CO systems (right, integration curve also included).

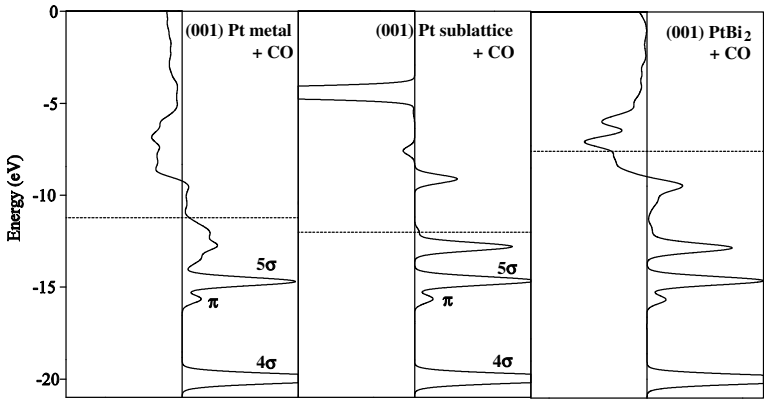

Fig. 9. COOP for the Pt–C bonds in (0 0 1) Pt metal + CO (left), (0 0 1) Pt sublattice + CO (middle) and (0 0 1) $PtBi_2$ + CO systems (right).

CO adsorption on the widely spaced (0 0 1) surface of the Pt sublattice in $PtBi_2$ (Fig. 8, 2nd panel). Since the Pt atoms are so far from each other in this sublattice, the CO–lattice interaction is actually reduced to the interaction just with the Pt atom directly underneath. As a result, the C–O and Pt–C COOP features are the same, only they involve more or less discrete levels instead of bands.

Finally, going to the real (0 0 1) $PtBi_2$ + CO system (Fig. 8, right), it can be seen that the shape of the analogous COOPs does not change much: the π* levels spread out more, while those that mix with the Pt d in a bonding way form a narrower (relative to the bulk Pt case) peaked band, more similar to the case of CO adsorption on the Pt sublattice. This is not unexpected, since the Bi atoms separate the Pt's, but do not participate in the direct Pt–CO interaction, their influence being seen just in the charge transfer.

The characteristic that essentially differentiates the three systems is the Fermi level and the electron filling of the bands. For the CO + Pt metal and Pt sublattice systems, all the C–O bonding levels are occupied, plus a small part of the CO π* levels, those which have mixed into the Pt d band. The latter is responsible for the slight to moderate weakening of the chemisorbed C–O bond with respect to the free CO molecule.

The situation is quite different for CO on the $PtBi_2$ surface: the π* antibonding levels are almost

completely filled, few of them being pushed above E_F by interaction with the Pt d_{xz} and d_{yz} orbitals. The net CO overlap population (OP) decreases dramatically (the integration actually becomes negative) and consequently CO is expected to dissociate upon adsorption. At the same time, the Pt–C COOP shows strong bonding interaction (net positive OP) in all three cases, though there is some occupation of Pt–C antibonding levels for CO on $PtBi_2$. The C–O and Pt–C bonds in the case of CO chemisorption on the Pt sublattice and Pt metal surfaces are very similar. Thus, from a bonding perspective, the important changes for CO adsorption on $PtBi_2$ relative to pure Pt are the electronic consequences of the "insertion" of Bi atoms into the Pt sublattice and not the "dilation" of the Pt metal structure (separation of Pt atoms).

These effects can be traced in further detail through an analysis of the occupation of CO fragment MOs (FMOs, Table 1). The electron flow from the 4σ and 5σ MOs is similar for all three cases: Pt metal, Pt sublattice (values not included) and $PtBi_2$ lattices, and proportional to their extent of interaction: around 0.2 and 0.3–0.4 electrons, respectively. The π* occupation, however, rises dramatically to 1.6–1.7 in CO on $PtBi_2$, compared to 0.2 in the Pt + CO systems.

On the other hand, the OP between each of the CO orbitals and Pt (summed over all occupied bands) does not change significantly on going from Pt metal to $PtBi_2$ (actual values given in the Supporting information), so that the overall strength of the Pt–C bond is similar for these two surfaces. The levels at the bottom of the π* band (the region from −11 eV to −9 eV in Fig. 9) have stronger bonding character in the $PtBi_2$ + CO case. However, due to the much higher Fermi level of the $PtBi_2$ slab with respect to Pt metal, electrons are dumped from the crystal into the lower lying empty MOs of CO in such a way that at the Fermi level the filling of some antibonding CO π*-Pt d orbitals approximately cancels out this difference. It appears that the major effect of the Bi atoms is to raise the Fermi level (E_F), and not a band shift triggered by Pt–Bi orbital interactions.

Table 1
Electron occupation of CO FMOs upon adsorption on (001) $PtBi_2$ surface

MO of CO	CO layer	$PtBi_2$ + CO	Pt metal + CO
π_y*	0	1.64	0.23
π_x*	0	1.71	0.23
5σ	2	1.70	1.62
π_y	2	2.00	2.00
π_x	2	2.00	2.00
4σ	2	1.82	1.81

6.2. Energetics of chemisorption

The total energy of adsorption was computed as the difference between the energy of the chemisorbed system and the sum of the energies of its separate components, the respective slab and the single CO layer:

$$E_{tot} = E_{slab+CO(ads.)} - (E_{slab} + E_{CO\ layer})$$

Thus a negative value of E_{tot} implies bonding.

The resulting adsorption energies for $PtBi_2$ (E_{tot} in Table 2) are highly and unrealistically negative (around −7 eV). This is caused by an "ionic" type

Table 2
Total (E_{tot}) and adjusted (E_{ads}) adsorption energies (eV) of atop CO on different $PtBi_2$ and Pt metal surfaces

$PtBi_2$ surface	(001)	(110)	(111)		
Adsorption site			*o*[a]	*m*[a]	*c*[a]
E_{tot}	−7.47	−6.08	−7.567	−7.651	−7.302
E_{ads}	−0.64	1.03	−0.839	−0.923	−0.574
Pt metal surface	(001)	(110)		(111)	
E_{tot}	−3.22	−3.53		−3.43	
E_{ads}	−3.22	−3.53		−3.43	

[a] *o*, *m* and *c* are distinct sites on the (111) $PtBi_2$ surface, as defined in Fig. 6.

of interaction particular to the eH methodology—since the energy levels do not adjust to the charge on the subsystem, electrons simply flow from $PtBi_2$ to CO, even at large separation. For this reason, the calculations were repeated for each slab with CO at 5 Å above the surface, where effectively there is no covalent interaction. By subtracting this "ionic component" from the energy of the real chemisorbed system (Pt–C distance: 1.85 Å) the result gives the effective "covalent" energy of interaction upon adsorption, which we call E_{ads}:

Table 3
Total (E_{tot}) and adjusted (E_{ads}) adsorption energies (eV) of CO on different PtBi surfaces

	(001)	(100)	(110)
PtBi surface—atop position			
E_{tot}	−6.89	−5.44	−4.58
E_{ads}	−1.16	−1.28	−0.39
PtBi surface—bridge position			
E_{tot}	–	−6.96	−5.63
E_{ads}	–	−2.80	−1.44

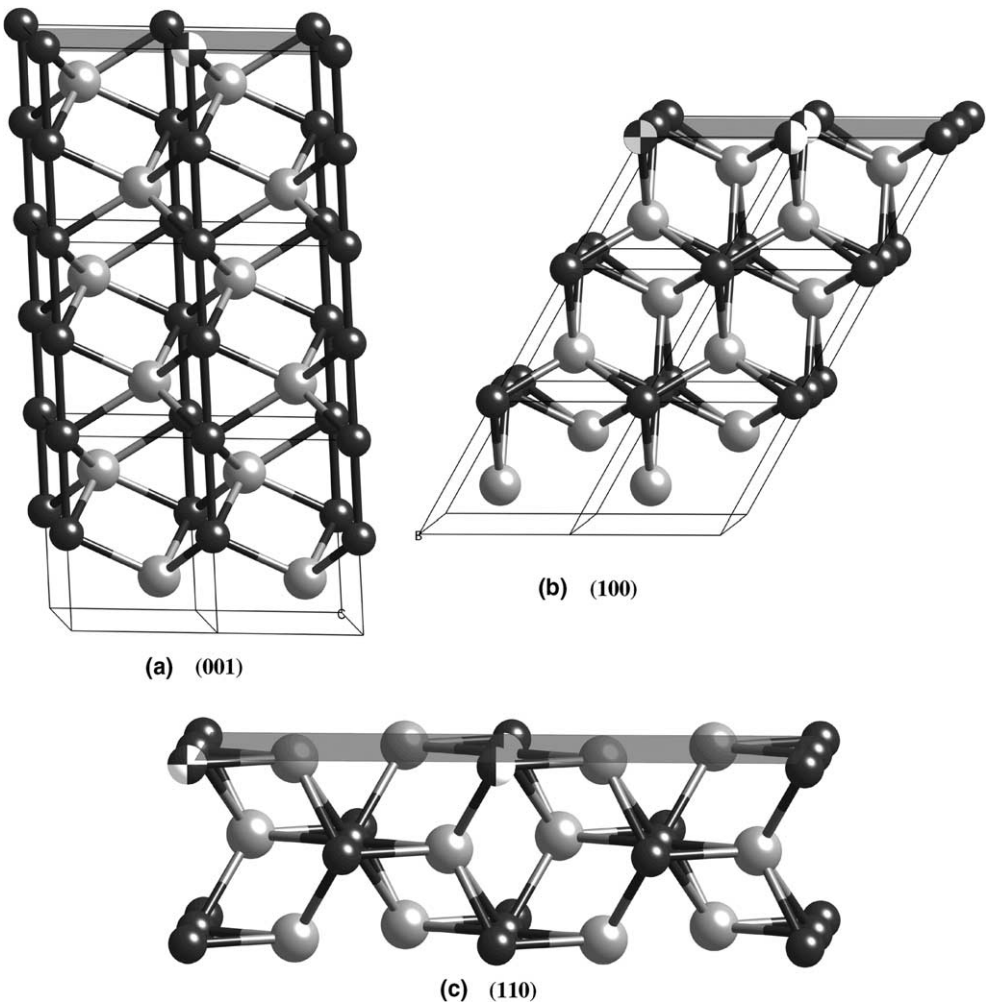

Fig. 10. Actual slabs and different adsorption sites (atop: quarter split; bridge: half split atoms) chosen for the adsorption of CO on PtBi surfaces (gray plane): (a) (001), (b) (100), (c) (110).

$$E_{ads} = E_{slab+CO(ads.)} - E_{slab+CO(not\ ads.,\ at\ 5\,\text{Å})}$$

For Pt metal (Table 2) and the Pt sublattice (values not shown), the two energies (E_{tot} and E_{ads}) are identical. For $PtBi_2$ an analogous factoring out of the electron flow leads to substantial changes. The energy of interaction goes down by ≈90% and even becomes unfavorable in the case of the (1 1 0) surface.

7. CO chemisorption on PtBi

The general features of the DOS of PtBi are very similar to $PtBi_2$. The Pt d band is centered around the same energy (−12.5 eV), with a dispersion of 1.5 eV—slightly less than in the previous compound. As expected, the adsorption energies in the atop position on different PtBi surfaces (Table 3)—depicted in Fig. 10 by quarter split atoms—are comparable with those for the $PtBi_2$ + CO system. There are differences in orbital interactions and bond strengths, but these are not worth a more detailed description.

The interesting changes come only from the possibility of CO adsorption in a bridge position on certain PtBi surfaces. The ones considered in our calculations are the (1 0 0) and (1 1 0) surfaces (non-equivalent bridge adsorption sites are presented in white in Fig. 10) and the results for these two are again similar to each other. Therefore, the following discussion will emphasize only the differences between the adsorption of CO on the (1 0 0) PtBi surface in the atop and bridge positions (surface top views in Fig. 11).

A comparison of the DOS and the CO FMOs contributions to the total DOS (not illustrated here) for atop and bridged chemisorption of CO on (1 0 0) PtBi shows small differences—in the bridged mode 4σ is shifted down a bit more and the π* band dispersion is somewhat greater. There is also a little less occupation of the CO π*. These trends are confirmed by FMO occupation analysis—there is a little more electron transfer out of 4σ (and 5σ) in the bridge site.

A point to be considered is why is there less occupation of CO π* in the bridging case? Actually Pt–CO interactions are larger (in part due to the fact that more Pt d levels at different *k*-points have the right symmetry to interact—see Fig. 12d and e). There is even some π-type mixing into the high-lying Pt p_z, due to combinations such as those shown in Fig. 12f.

Fig. 13 compares the COOP of the C–O bonds in the CO layer (left), PtBi + CO atop (middle) and PtBi + CO bridged (right) systems. The net C–O OP in the latter is somewhat larger than in the atop chemisorption case because the increased

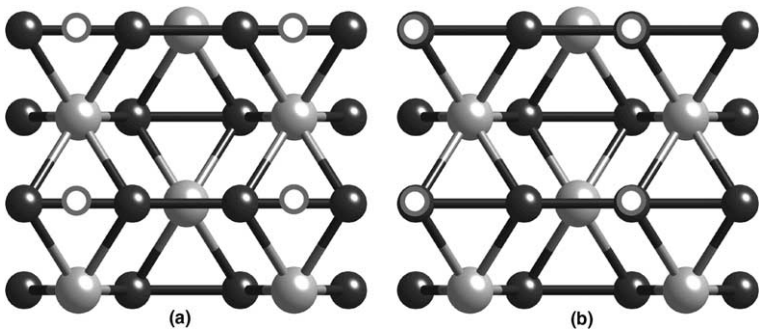

Fig. 11. Top view of the (1 0 0) PtBi surface covered with chemisorbed CO (C: small gray; O: white atoms; shown in projection, so C and O appear as overlapping circles) in the (a) bridge and (b) atop position. The figures also show the three layers underneath the surface: first two are Bi layers and the last one—a Pt layer (formed by the Pt atoms in the horizontal rows that do not contain any CO).

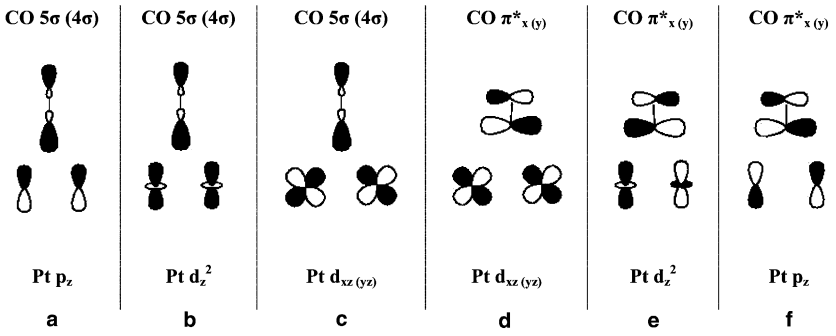

Fig. 12. Possible Pt–CO orbital interactions for the adsorption of CO between two Pt atoms: (a)–(c) σ type and (d)–(f) π type overlaps. CO 4σ has the same orbital topology as 5σ, but with O mixed in an out-of-phase fashion.

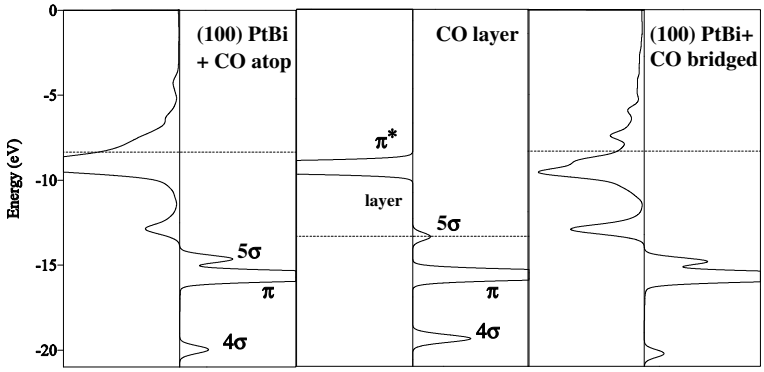

Fig. 13. COOP for the C–O bonds in (1 0 0) PtBi + CO atop (left), CO isolated layer (middle) and (1 0 0) PtBi + CO bridged (right).

spreading of the π* band pushes a significant part of the levels above E_F. Instead, the Pt–C OP is smaller than for the atop adsorption site, presumably due to the loss in σ type overlap. On the other hand, the Pt–Pt surface bond is significantly weakened upon chemisorption (slightly negative OP: −0.03, compared to 0.28 in the surface without CO), while in the PtBi + CO atop case the bond is just weakened somewhat (OP: 0.19). The Pt–Pt bond weakening is due to occupation of combinations such as in Fig. 12d–f. The Pt–C bond forms also at the expense of the surface Pt to Bi interactions. Most affected are the bonds between the adsorption site Pt and the Bi atoms in the first two layers below the surface, while all other bonds remain virtually unaffected.

Table 4
Overlap populations between CO orbitals and Pt

OP	PtBi + CO atop	PtBi + CO bridged
π_y*-Pt	0.15	0.17
π_x*-Pt	0.12	0.26
5σ-Pt	0.39	0.19
4σ-Pt	0.20	0.10

The σ type overlap between CO and Pt is not very good (the OP decreases to half the value for the atop chemisorption; see Table 4 and Fig. 12a–c), while the π type overlap increases

considerably (from 0.12 and 0.15 to 0.26 and 0.17, respectively). These numbers include the π-type interaction of the CO σ MOs at some *k*-points (Fig. 12e and f). The analysis of the occupation of Pt levels only confirmed the more extensive spreading of the Pt $p_{x,y,z}$ towards higher energies, due to the mixing with the CO π* band.

The smaller extent of back donation into the CO π*, and the stronger Pt–CO orbital interactions result in significantly more favorable adsorption energies for the bridge position (Table 3).

8. Conclusions

The approximate MOs calculations show that, generally, the propensity for CO adsorption is drastically reduced on all $PtBi_2$ and PtBi surfaces with respect to bulk Pt, reflecting the experimental findings of Abruña and co-workers [56]. The chemisorption energies for CO on $PtBi_2$ are between 18% and 27% of the values for the corresponding metallic Pt surfaces, calculated with the same method, while on PtBi the CO chemisorption is somewhat more favorable in the atop position and to a larger extent in a bridge geometry. This can explain the very low CO poisoning of the PtBi electrode observed by Abruña and co-workers in their experiments [56].

Regarding the way CO binds to the surface, the orbital interactions involved are similar in both pure Pt and Pt–Bi compounds. The main changes are caused indirectly by the Bi atoms, which by raising the Fermi level of the system, determine the occupation of higher-lying antibonding orbitals, especially C–O. What the experimental studies do not support is the theoretically predicted dissociation of CO upon adsorption; there is no evidence of such a process at the Pt–Bi electrodes. Perhaps the extended Hückel method overestimates the degree of electron transfer to CO π*. Since the CO poisoning experiments performed in the Abruña group show that the phenomenon is not completely inhibited by the presence of the Bi atoms [56], it cannot be the case that the adsorption energies are actually unfavorable for all surfaces. It may be that the mechanism of oxidation of formic acid through the reactive intermediate is selectively promoted by the intermetallic electrode, and CO does not form to such an extent as to allow the observation of dissociation products.

Further, higher level (DFT) calculations are necessary in order to verify this qualitative picture of bonding and to provide accurate data about the energetics and preferred position for CO adsorption on Pt–Bi bulk alloy surfaces.

Acknowledgment

We are grateful to Mihaela D. Bojin, Beate Flemmig and Emerilis Casado-Rivera for helpful discussions, and to National Science Foundation for its support of our research through grant CHE 0204841.

Supplementary material

Supplementary data associated with this article can be found, in the online version, at doi:10.1016/j.susc.2004.09.045.

Appendix A

See Table 5.

Table 5
Extended Hückel method parameters used in the calculations: exponents of the STOs (Exp), Coulomb integrals (H_{ii}) and coefficients of the STOs used in the expansion of d-type orbitals (Coef)

Atom	Exp-s	H_{ii}-s	Exp-p	H_{ii}-p	Exp1-d	Exp2-d	H_{ii}-d	Coef1-d	Coef2-d
Pt	2.554	−9.080	2.554	−5.470	6.013	2.696	−12.590	0.6334	0.5513
Bi	2.653	−15.750	2.092	−10.520					
C	1.625	−21.400	1.625	−11.400					
O	2.275	−32.300	2.275	−14.800					

References

[1] A. Gil, A. Clotet, J.M. Ricart, G. Kresse, M. García-Hernández, N. Rösch, P. Sautet, Surf. Sci. 530 (2003) 71, and references therein.
[2] R.A. Olsen, P.H.T. Philipsen, E.J. Baerends, J. Chem. Phys. 119 (2003) 4522.
[3] I. Grinberg, Y. Yourdshahyan, A.M. Rappe, J. Chem. Phys. 117 (2002) 2264.
[4] P.J. Feibelman, B. Hammer, J.K. Nørskov, F. Wagner, M. Scheffler, R. Stumpf, R. Watwe, J. Dumesic, J. Phys. Chem. B 105 (2001) 4018.
[5] M. Lynch, P. Hu, Surf. Sci. 458 (2000) 1.
[6] S.C. Creighan, R.J. Mukerji, A.S. Bolina, D.W. Lewis, W.A. Brown, Catal. Lett. 88 (2003) 39.
[7] A.D. Karmazyn, V. Fiorin, S.J. Jenkins, D.A. King, Surf. Sci. 538 (2003) 171.
[8] M. Kinne, T. Fuhrmann, C.M. Whelan, J.F. Zhu, J. Pantförder, M. Probst, G. Held, R. Denecke, H.-P. Steinrück, J. Chem. Phys. 117 (2002) 10852.
[9] M. Nowicki, A. Emundts, G. Pirug, H.P. Bonzel, Surf. Sci. 478 (2001) 180.
[10] B.H. Choi, A.P. Graham, K.T. Tang, J.P. Toennies, J. Chem. Phys. 112 (2000) 10538.
[11] X. Su, P.S. Cremer, Y.R. Shen, G.A. Somorjai, Phys. Rev. Lett. 77 (1996) 3858.
[12] J. Liu, M. Xu, T. Nordmeyer, F. Zaera, J. Phys. Chem. 99 (1995) 6167.
[13] J. Xu, J.T. Yates Jr., Surf. Sci. 327 (1995) 193.
[14] R. Martin, P. Gardner, A.M. Bradshaw, Surf. Sci. 342 (1995) 69.
[15] T. Gritsch, D. Coulman, R.J. Behm, G. Ertl, Phys. Rev. Lett. 63 (1989) 1086.
[16] I.M. Ciobîcă, A.W. Kleyn, R.A. van Santen, J. Phys. Chem. B 107 (2003) 164.
[17] I.V. Yudanov, R. Sahnoun, K.M. Neyman, N. Rösch, J. Chem. Phys. 117 (2002) 9887.
[18] F. Favot, A.D. Corso, A.J. Baldereschi, Chem. Phys. 114 (2001) 483.
[19] W.V. Glassey, R. Hoffmann, J. Phys. Chem. B 105 (2001) 3245.
[20] S.K. Nayak, M. Nooijen, S.L. Bernasek, J. Phys. Chem. B 105 (2001) 164.
[21] S.A. Wasileski, M.T.M. Koper, M.J. Weaver, J. Phys. Chem. B 105 (2001) 3518.
[22] Q. Ge, S.J. Jenkins, D.A. King, Chem. Phys. Lett. 327 (2000) 125.
[23] B. Hammer, L.B. Hansen, J.K. Nørskov, Phys. Rev. B 59 (1999) 7413.
[24] G. Pacchioni, S.-C. Chung, S. Krüger, N. Rösch, Surf. Sci. 392 (1997) 173.
[25] P. Hu, D.A. King, S. Crampin, M.-H. Lee, M.C. Payne, J. Chem. Phys. 107 (1997) 8103.
[26] R. Ramprasad, K.M. Glassford, J.B. Adams, R.I. Masel, Surf. Sci. 360 (1996) 31.
[27] M. Nygren, P.E.M. Siegbahn, J. Phys. Chem. 96 (1992) 7579.
[28] W. Müller, P.S. Bagus, J. Vac. Sci. Technol. A 3 (1985) 1623.
[29] A.B. Anderson, M.K. Awad, JACS 107 (1985) 7854.
[30] S.-S. Sung, R. Hoffmann, JACS 107 (1985) 578.
[31] P.S. Bagus, K. Hermann, C.W. Bauschlicher Jr., J. Chem. Phys. 81 (1984) 1966.
[32] J.W. Allison, W.A. Goddard III, Surf. Sci. 115 (1982) 553.
[33] A. Föhlisch, M. Nyberg, P. Bennich, L. Triguero, J. Hasselström, O. Karis, L.G.M. Pettersson, A. Nilsson, J. Chem. Phys. 112 (2000) 1946, and references therein.
[34] J. Lahtinen, J. Vaari, K. Kauraala, E.A. Soares, M.A. Van Hove, Surf. Sci. 448 (2000) 269.
[35] P. Sautet, M.K. Rose, J.C. Dunphy, S. Behler, M. Salmeron, Surf. Sci. 453 (2000) 25.
[36] Y.Y. Yeo, L. Vattuone, D.A. King, J. Chem. Phys. 106 (1997) 1990.
[37] R. Davis, D.P. Woodruff, P. Hofmann, O. Schaff, V. Fernandez, K.-M. Schindler, V. Fritzsche, A.M. Bradshaw, J. Phys. Condens. Mat. 8 (1996) 1367.
[38] W. Wurth, C. Schneider, R. Treichler, E. Umbach, D. Menzel, Phys. Rev. B 35 (1987) 7741.
[39] E.S. Jensen, T.N. Rhodin, Phys. Rev. B 27 (1983) 3338.
[40] M.T.M. Koper, T.E. Shubina, R.A. van Santen, J. Phys. Chem. B 106 (2002) 686.
[41] Y. Ishikawa, M.-S. Liao, C.R. Cabrera, Surf. Sci. 513 (2002) 98.
[42] F. Delbecq, P. Sautet, Phys. Rev. B 59 (1999) 5142.
[43] A.B. Anderson, E.J. Grantscharova, Phys. Chem. 99 (1995) 9149.
[44] A. Schlapka, M. Lischka, A. Groß, U. Käsberger, P. Jakob, Phys. Rev. Lett. 91 (2003) 016101.
[45] V.R. Stamenković, M. Arenz, C.A. Lucas, M.E. Gallagher, P.N. Ross, N.M. Marković, JACS 125 (2003) 2736.
[46] G.F. Cabeza, P. Légaré, N.J. Castellani, Surf. Sci. 465 (2000) 286.
[47] C. Panja, M.E. Jones, J.M. Heitzinger, S.C. Gebhard, B.E. Koel, J. Phys. Chem. B 104 (2000) 3130.
[48] M.Ø. Pedersen, S. Helveg, A. Ruban, I. Stensgaard, E. Lægsgaard, J.K. Nørskov, F. Besenbacher, Surf. Sci. 426 (1999) 395.
[49] C. Becker, T. Pelster, M. Tanemura, J. Breitbach, K. Wandelt, Surf. Sci. 427–428 (1999) 403.
[50] T. Iwasita, Electrochim. Acta 47 (2002) 3663.
[51] P. Costamagna, S.J. Srinivasan, Power Sources 102 (2001) 242.
[52] G.T. Burnstein, C.J. Barnett, A.R. Kucernak, K.R. Williams, Catal. Today 38 (1997) 425.
[53] A. Hammer, Catal. Today 38 (1997) 445.
[54] R. Parsons, T.J. VanderNoot, Electroanal. Chem. 257 (1988) 9.
[55] B. Beden, C. Lamy, N.R. De Tacconi, A. Arvia, J. Electrochim. Acta 35 (1990) 691.
[56] E. Casado-Rivera, Z. Gal, A.C.D. Angelo, C. Lind, F.J. DiSalvo, H.D. Abruña, Chem. Phys. Chem. 4 (2003) 193.
[57] A. Capon, R. Parsons, Electroanal. Chem. Interfacial Electrochem. 45 (1973) 205.
[58] M. Breiter, Electrochim. Acta 12 (1967) 1213.
[59] G.J. Blyholder, Phys. Chem. 68 (1964) 2772.

[60] A. Fölisch, M. Nyberg, J. Hasselström, O. Karis, L.G.M. Pettersson, A. Nilsson, Phys. Rev. Lett. 15 (2000) 3309.
[61] L. Ford, P. Blowers, N. Chen, I. Lee, R. Masel, Surf. Sci. 419 (1999) 144.
[62] D. Curulla, A. Clotet, J.M. Ricart, F. Illas, J. Phys. Chem. B 103 (1999) 5246.
[63] H. Aizawa, S. Tsuneyuki, Surf. Sci. 399 (1998) L364.
[64] G. Rangelov, N. Memmel, E. Bertel, V. Dose, Surf. Sci. 251–252 (1991) 965.
[65] Y.-T. Wong, R. Hoffmann, J. Phys. Chem. 95 (1991) 859.
[66] G. Pacchioni, P.S. Bagus, J. Chem. Phys. 93 (1990) 1209.
[67] D. Post, E.J. Baerends, J. Chem. Phys. 78 (1983) 5663.
[68] S.R. Bare, K. Griffiths, P. Hofmann, D.A. King, G.L. Nyberg, N.V. Richardson, Surf. Sci. 120 (1982) 367.
[69] N.N. Zhuravlev, A.A. Stepanova, Sov. Phys.-Crystallogr. 7 (1962) 241.
[70] M.G. Morgan, M. Wang, W.Y. Chan, A. Mar, Inorg. Chem. 42 (2003) 1549, and references therein.
[71] M.G. Haase, H. Block, W. Jeitschko, Z. Anorg. Allg. Chem. 627 (2001) 1941.
[72] F. Gascoin, S.C. Sevov, JACS 122 (2000) 10251, and references therein.
[73] N.E. Brese, H.G. von Schnering, Z. Anorg. Allg. Chem. 620 (1994) 393.
[74] G.A. Landrum, W.V. Glassey, YAeHMOP: Yet Another extended Hückel Molecular Orbital Package Version 2.0b 1999. http://sourceforge.net/projects/yaehmop/.
[75] C. Mealli, D.M. Proserpio, J. Chem. Educ. 67 (1990) 399.
[76] M. Mavrikakis, B. Hammer, J.K. Nørskov, Phys. Rev. Lett. 81 (1998) 2819.
[77] B. Hammer, O.H. Nielsen, J.K. Nørskov, Catal. Lett. 46 (1997) 31.
[78] A. Ruban, B. Hammer, P. Stoltze, H.L. Skriver, J.K.L. Nørskov, Mol. Catal. A: Chem. 115 (1997) 421.
[79] B. Hammer, Y. Morikawa, J.K. Nørskov, Phys. Rev. Lett. 76 (1996) 2141.
[80] B. Hammer, J.K. Nørskov, Surf. Sci. 343 (1995) 211.
[81] B.N.J. Persson, M. Tüshaus, A.M. Bradshaw, J. Chem. Phys. 92 (1990) 5034.
[82] M. Kiskinova, A. Szabó, J.T. Yates Jr., Surf. Sci. 205 (1988) 215.
[83] D.A. Wesner, F.P. Coenen, H.P. Bonzel, J. Vac. Sci. Technol., A 5 (1987) 927.
[84] D. Rieger, R.D. Schnell, W. Steinmann, Surf. Sci. 143 (1984) 157.
[85] S.R. Bare, P. Hofmann, D.A. King, Surf. Sci. 144 (1984) 347.
[86] G.S. Blackman, M.-L. Xu, D.F. Ogletree, M.A. van Hove, G.A. Somorjai, Phys. Rev. Lett. 61 (1988) 2352.
[87] D.F. Ogletree, M.A. van Hove, G.A. Somorjai, Surf. Sci. 173 (1986) 351.
[88] T. Hughbanks, R. Hoffmann, JACS 105 (1983) 3528.